Vibrational properties of ZnTe at high pressures

2002 J. Phys.: Condens. Matter 14 739

(http://iopscience.iop.org/0953-8984/14/4/309)

INSTITUTE OF PHYSICS PUBLISHING JOURNAL OF PHYSICS: CONDENSED MATTER

J. Phys.: Condens. Matter **14** (2002) 739–757 PII: S0953-8984(02)30215-7

Vibrational properties of ZnTe at high pressures

J Camacho[1,2,3], I Loa[1], A Cantarero[2] and K Syassen[1]

[1] Max-Planck-Institut für Festkörperforschung, Heisenbergstrasse 1, D-70569 Stuttgart, Germany
[2] Instituto de Ciencia de Materiales, Universidad de Valencia, PO Box 22085, E-46071 Valencia, Spain

E-mail: Juana.Camacho@uv.es

Received 15 October 2001
Published 18 January 2002
Online at stacks.iop.org/JPhysCM/14/739

Abstract

Raman spectra of ZnTe were measured under hydrostatic pressures up to 15 GPa at $T = 300$ K. Results for the frequencies of first- and second-order Raman features of the zincblende phase (0–9.5 GPa) are used to set up a rigid-ion model of the phonon dispersion relations under pressure. Calculated phonon densities of states, mode Grüneisen parameters and the thermal expansion coefficient as a function of pressure are discussed. The effect of pressure on the widths and intensities of Raman spectral features is considered. Raman spectra of high-pressure phases of ZnTe are reported. These spectra indicate the possible existence of a new phase near 13 GPa, intermediate between the cinnabar and orthorhombic ($Cmcm$) phases of ZnTe.

(Some figures in this article are in colour only in the electronic version)

1. Introduction

Zinc telluride at ambient conditions is a semiconductor with zincblende (ZB) crystal structure and a fundamental direct energy gap in the visible spectral range (2.3 eV at 300 K). Similar to other tetrahedral semiconductors [1], the effect of pressure on the physical properties of ZB-ZnTe has been the subject of numerous experimental and theoretical investigations. The vibrational properties of ZB-ZnTe under pressure have been studied in the past using Raman spectroscopy [2–7]. The first-order Raman scattering of a ZB-type crystal usually consists of two features corresponding to the transverse optic (TO) and longitudinal optic (LO) zone-centre phonon modes. The second-order Raman scattering of ZnTe, by combinations of phonons with total wavevector $\vec{q} = 0$, provides additional information on phonon mode frequencies at critical points near the edge of the first Brillouin zone (BZ). Based on the phonon dispersions of ZnTe at ambient conditions from inelastic neutron scattering [8] and pressure-dependent Raman measurements of ZB-ZnTe, Weinstein [4] proposed a semi-quantitative picture of the effect of

[3] Author to whom any correspondence should be addressed.

pressure on the dispersion relations along high-symmetry directions of the BZ. Subsequently, a rigid-ion model (RIM) [9] was used to calculate phonon dispersions at a fixed pressure of 9.5 GPa by applying proper adjustments to the model parameters, partly based on experimental Raman data [10].

The ZB phase of ZnTe is stable up to ∼9.5 GPa. Three high-pressure phases of ZnTe are known to exist at 300 K [11–26]. With increasing pressure ZnTe first transforms to a semiconducting cinnabar-type phase [16–21], followed by a transition to a metallic orthorhombic (*Cmcm*) phase at about 12 GPa [22]. The structure of the latter phase, which transforms to an as yet unidentified phase at about 85 GPa, [23] can be viewed as a distorted rocksalt lattice. A NaCl-type high-pressure modification of ZnTe was observed only at elevated temperatures [27]. The stability of ZnTe in various crystal structures has been investigated theoretically using microscopic models [28–30]. The theoretical results are in overall agreement with the observed structural behaviour at room temperature.

In this paper we report Raman scattering measurements of ZB-ZnTe at hydrostatic pressures up to ∼9.5 GPa at $T = 300$ K. The observed first- and second-order Raman features are used to derive pressure-dependent RIM parameters for the phonon dispersion relations. The model is then applied to calculate the effect of pressure on phonon-related properties, including the anomalous negative thermal expansion at low temperatures, and to consider intrinsic mechanisms leading to different widths of the first-order TO and LO Raman peaks. We observed pronounced pressure-induced changes of the first- and second-order Raman intensities and offer qualitative explanations.

In addition, we report here Raman spectra of the cinnabar and *Cmcm* phases of ZnTe. The Raman data indicate the possible existence of a new high-pressure phase intermediate between cinnabar and *Cmcm*.

2. Experimental details

Single-crystal samples with thicknesses of ∼30 μm were cut into pieces of about 100 × 100 μm^2 in size in order to fit into the gasket of a diamond anvil high-pressure cell (DAC). The experiments were carried out at room temperature. The pressure medium was a 4:1 methanol–ethanol mixture. Pressures were measured by the ruby luminescence method [31]. Raman experiments were performed in back-scattering geometry using the 647.088 nm line of a Kr^+ ion laser, focused down to a 30 μm spot on the sample. At all pressures, the laser energy (1.92 eV) lies below the fundamental bandgap energy of ZB-ZnTe. The incident laser power was kept below 5 mW. The scattered light was analysed with a Jobin-Yvon T64000 triple-grating spectrometer in the subtractive dispersion mode using a multi-channel detector (CCD camera). Most of the spectra were taken without a polarization analyser. The spectral resolution was 0.6 cm^{-1}.

3. Zincblende phase

3.1. Experimental results

Raman spectra of ZB-ZnTe are shown in figure 1. Besides the Raman peaks corresponding to the TO and LO modes at the Γ-point, several two-phonon features corresponding to different wavevectors in the BZ are clearly observed. In the low-frequency region, we can find the structures related to 2TA(L), 2TA(X) and 2TA$_2$(K) scattering. Above the LO(Γ) region, a double structure, related to the LO(L) + TA(L) and LO(X) + TA(X) contributions is also observed. The inset in figure 1 depicts this spectral region (225–270 cm^{-1}) at 2.3 GPa. The assignments of all peaks are consistent with ambient-pressure Raman data [32], inelastic neutron scattering measurements [8] and previous Raman investigations of ZnTe under pressure [4].

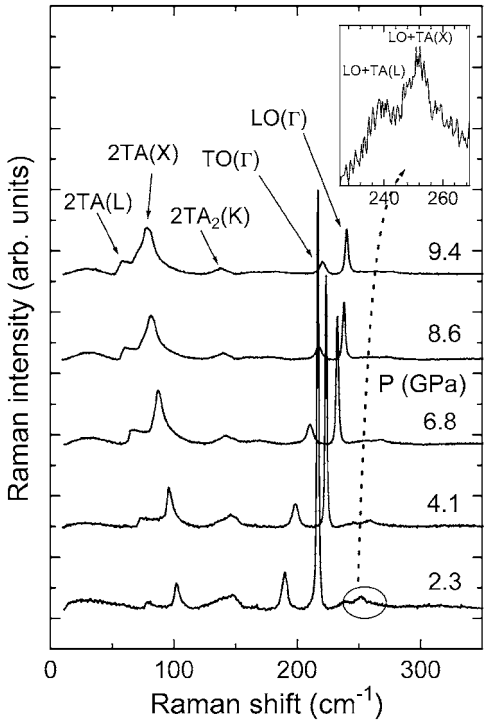

Figure 1. Raman spectra of ZB-ZnTe at different pressures ($T = 300$ K). The spectra shown here were measured for increasing pressure. The laser wavelength was 647.088 nm. All spectra are normalized to the same exposure time.

In figure 2 we have plotted the frequencies of Raman features as a function of pressure. In the optical mode region the frequencies of the Raman modes increase with pressure, while for the purely acoustic overtones the behaviour is the opposite. In the combinations of acoustic and optical modes, the pressure-induced shift of the optical modes dominates. The softening of the zone-edge TA phonons with increasing pressure is common to most tetrahedral cubic semiconductors (diamond being an exception) [33, 34]. The sign of the pressure dependence of the phonon frequencies in tetrahedral semiconductors depends on a balance between central and non-central elastic forces associated with the stretching and bending of bonds. For the shear-type zone-boundary TA modes the angular forces tend to make the mode stiffer under pressure, but central elastic forces act in the opposite way, resulting in a mode softening [35].

In figure 2 the pressure dependence is essentially linear for the acoustic modes, while in the case of the optic modes a parabolic fit is more appropriate. The phonon frequencies and their pressure coefficients are listed in table 1.

The scaling of a phonon frequency ω_i with volume is described by the Grüneisen parameter γ, which may depend on the pressure P:

$$\gamma_i(\vec{q}, P) = -\left[\frac{\mathrm{d}\ln\omega_i(\vec{q})}{\mathrm{d}\ln V}\right]_{V(P)} = \frac{B_T(P)}{\omega_i(\vec{q}, P)}\left[\frac{\partial\omega_i(\vec{q}, P)}{\partial P}\right]_T. \tag{1}$$

We have converted our linear pressure coefficients (cf table 1) to Grüneisen parameters using $B_0 = 48.0$ GPa for the ambient-pressure isothermal bulk modulus $B_T(0)$ [15]. It should be noted that this value agrees quite well with the adiabatic bulk modulus of 50.8 GPa derived from the experimental values of the elastic compliances c_{ij} [36]. The experimental mode

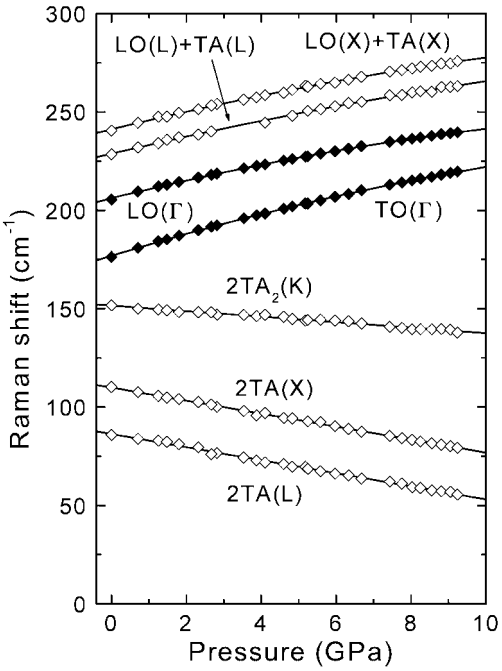

Figure 2. Observed Raman frequencies of ZB-ZnTe as a function of pressure ($T = 300$ K). The assignment of Raman features to one- and two-phonon combinations is indicated in the figure and explained in the text. The curves refer to fits using linear or quadratic polynomials.

Grüneisen parameters for seven phonons are listed in table 1, together with data taken from the literature [2–7, 37]. In general, our experimental result for a given mode falls into the interval spanned by the scatter in the literature data, except for the TA(L) mode, which is found to be slightly softer than reported previously.

The splitting of the LO and TO modes at Γ decreases with increasing pressure. This behaviour is related to the decrease of Born's transverse dynamic effective charge e^* given by [38]

$$e^* = \left[\frac{\epsilon_\infty \mu V_\mathrm{m}}{4\pi}(\omega_\mathrm{LO}^2 - \omega_\mathrm{TO}^2)\right]^{1/2}. \tag{2}$$

The quantities μ and V_m are the reduced effective mass and volume per formula unit, respectively, and ϵ_∞ is the electronic dielectric constant in the infrared spectral range. For ZnTe at ambient pressure we obtain $e^* = 2.02$, using $\epsilon_\infty = 7.28$. The Grüneisen parameter of e^* is

$$\begin{aligned}\gamma^* &= -\frac{\mathrm{d}\ \ln\ e^*}{\mathrm{d}\ \ln\ V} \\ &= \gamma_\mathrm{LO} + \frac{(\gamma_\mathrm{LO} - \gamma_\mathrm{TO})\omega_\mathrm{TO}^2}{\omega_\mathrm{LO}^2 - \omega_\mathrm{TO}^2} + \frac{1}{2}\gamma_\infty - \frac{1}{2}.\end{aligned} \tag{3}$$

The value of $\gamma_\infty = -\mathrm{d}\ \ln\ \epsilon_\infty/\mathrm{d}\ \ln\ V$ given in [33] is -0.6. From equation (3) and the Grüneisen parameters of table 1 we obtain $\gamma^* \simeq -1.03$. This value is slightly larger than typical values found for the III–V compounds ($\gamma^* \simeq -0.6$ for InP; see [34]). The negative sign, which corresponds to a decrease of the ionicity with decreasing volume, is reported for most tetrahedrally coordinated polar semiconductors [33, 34], SiC and GaN being exceptions [39, 40].

Table 1. Raman frequencies, pressure coefficients and ambient-pressure Grüneisen parameters of ZnTe. The γ_{exp} values refer to experimental mode Grüneisen parameters, while γ_{RIM} are calculated using the RIM (see text). Other experimental values from the literature (γ_{lit}) are given for comparison. Errors in frequencies and pressure coefficients are estimated values. Uncertainties in the bulk modulus value are not taken into account when converting from experimental pressure coefficients to Grüneisen parameters.

Mode	ω (cm^{-1})	$d\omega/dP$ (cm^{-1} GPa^{-1})	$\frac{1}{2}d^2\omega/dP^2$ (cm^{-1} GPa^{-2})	γ_{exp}	γ_{RIM}	γ_{lit}
TA(L)	43.1(4)	−1.66(6)	—	−1.85(6)	−2.09	1.0[a], −1.1[b], −1.64[c], 1.7[f]
TA(X)	55.0(4)	−1.66(6)	—	−1.47(5)	−1.42	−1.55[a], −1.1[b], −1.31[c]
TA_2(K)	75.8(4)	−0.70(6)	—	−0.44(4)	−0.44	−0.4[a], −0.20[c], −0.20[f]
TO(Γ)	176.9(5)	5.82(18)	−0.13(1)	1.58(5)	1.61	1.7[a], 1.6[b], 1.78[c], 1.55[d], 1.64[e]
LO(Γ)	206.1(5)	4.74(15)	−0.12(5)	1.10(3)	1.14	1.2[a], 1.15[c], 1.0[d], 1.08[e]
LO(L)	185.4(10)	6.30(45)	−0.10(3)	1.63(11)	1.75	1.8[a]
LO(X)	186.2(20)	6.32(33)	−0.10(3)	1.63(8)	1.68	1.7[a], 1.67[c]

[a] [4].
[b] [3].
[c] [5].
[d] [2].
[e] [7].
[f] [37]; calculated.

The widths of the TO and LO Raman features of ZnTe are found to be quite different. Figure 3 shows the full width at half maximum (FWHM) of Lorentzians fitted to the experimental data (no deconvolution made with the spectrometer function, a Gaussian of about 0.6 cm^{-1} FWHM). The LO peak width remains nearly constant up to about 5 GPa and then starts to broaden slightly at higher pressures. The TO feature, being much broader than the LO peak at ambient pressure, increases further in width up to 5 GPa and then remains nearly constant. The changes in line width are fully reversible when the pressure is released. This indicates that the pressure effects are not related to the stress-induced formation of defects.

Another experimental observation is (see figure 1) that the intensities of the first-order TO and LO Raman features and the acoustic two-phonon scattering below about 150 cm^{-1} change considerably with pressure. In figure 4(a) we have plotted the integrated TO and LO intensities as a function of pressure. The LO intensity decreases by more than one order of magnitude between 0 and 9.5 GPa, while for the TO mode the decrease is somewhat smaller. In contrast the two-phonon scattering intensity (figure 4(b)) increases with pressure. The observed intensity changes are reversible, but only in a qualitative sense. The reason is that reliable pressure-dependent intensity measurements in a DAC are difficult due to changes in the scattering conditions. A slight reorientation of the sample, although not evident from visual observation, cannot be ruled out. Due to changes in optical reflection effects, the Raman scattering at laser energies below the bandgap is a variable mixture of back- and forward scattering, such that selection rules are not strictly applicable. Nevertheless, the overall trends observed for the intensity variations as a function of pressure are much larger than these possible experimental artifacts.

3.2. Phonon dispersions and densities of states

The RIM of Kunc [41] provides a basis for discussing the effect of pressure on phonon-related properties which depend on phonon frequencies only and do not require us to consider phonon eigenvectors. The RIM parameters are two first-neighbour force constants (A and B), eight second-neighbour force constants (C_i, D_i, E_i and F_i, $i = 1, 2$, where in our case the indices 1

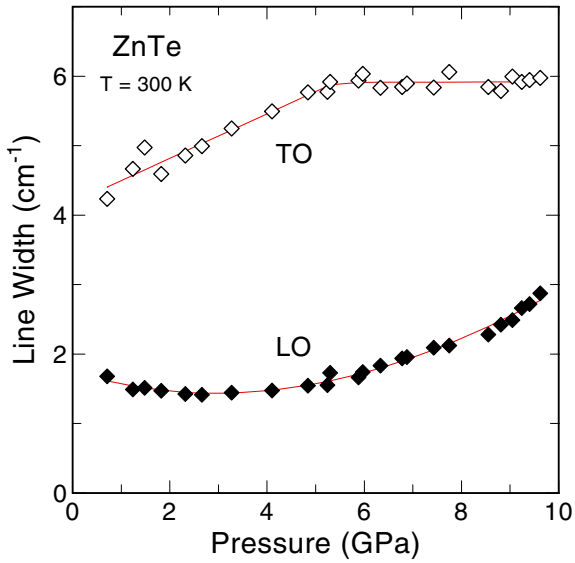

Figure 3. FWHM of the first-order TO and LO Raman peaks of ZnTe as a function of pressure ($T = 300$ K). Solid curves are guides to the eye.

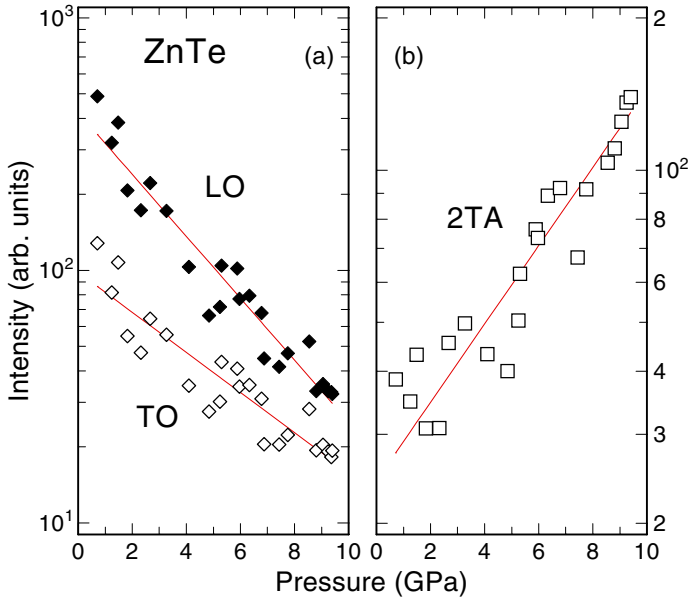

Figure 4. Integrated intensities of Raman features of ZnTe as a function of pressure: (a) the first-order TO and LO Raman peaks and (b) the two-phonon acoustic scattering. The solid lines are guides to the eye.

and 2 represent cations (Zn) and anions (Te), respectively) and the effective charge parameter $Z = e^*/\sqrt{\varepsilon_\infty}$. We have basically followed the prescriptions given in [9] and [10] to determine RIM parameters at ambient pressure and 9 GPa, based on Raman mode frequencies, ambient-pressure elastic constants and their extrapolated high-pressure values. Only minor changes

Table 2. Parameters ξ used in the RIM calculations at 0 and 9 GPa (see text for explanations) and parameters m_ξ used for interpolation (see equation (4)).

P (GPa)	A	B	C_1	C_2	D_1	D_2	E_1	E_2	F_1	F_2	Z
0	−0.223	−0.238	−0.0215	−0.033	−0.038	−0.0091	0.0513	−0.062	0.071	−0.082	0.748
9	−0.325	−0.354	−0.0465	−0.049	−0.074	−0.0263	0.0801	−0.063	0.120	−0.114	0.637
m_ξ				−11.23	−21.72	−43.90	13.3	−0.35	6.07	−9.10	

Table 3. Experimental and calculated values of the elastic constants (in GPa) of ZnTe. Also listed are the experimental pressure coefficients, from which the mode Grüneisen parameters of the zone-centre LA, TA(2) and TA(1) modes can be obtained (corresponding to c_{11}, c_{44} and $(c_{11} - c_{12})/2$, respectively).

		Experiment[a]		Calculated c_{ij} (RIM)		
	Related to	c_{ij} (0 GPa)	$\mathrm{d}c_{ij}/\mathrm{d}P$	0 GPa	4.5 GPa	9 GPa
c_{11}	LA	71.1(3)	4.81(7)	73.2	98.8	122.0
c_{12}		40.7(4)	5.12(1)	40.8	69.7	95.2
c_{44}	TA(2)	31.3(2)	0.45(3)	30.8	33.9	33.1
$(c_{11} - c_{12})/2$	TA(1)	15.2(7)	−0.15(8)	16.2	14.55	13.40

[a] [36].

in some parameter values were introduced (e.g. for B, C_1, E_1 and Z at ambient pressure) in order to better fit our Raman data. Parameters A, B, C_1 and Z can be evaluated directly from our Raman data as a function of pressure (see [9]). The other RIM parameters at pressures intermediate between 0 and 9 GPa are interpolated assuming a linear variation of a given parameter ξ with bond distance [42]

$$\frac{\Delta\xi(P)}{\xi_0} = m_\xi \frac{\Delta r(P)}{r_0}. \tag{4}$$

The value of the ambient-pressure cubic lattice constant is 6.1037 Å, i.e. r_0 is 2.6429 Å. The variation of r with pressure is obtained using a Murnaghan relation [43] for the pressure–volume relation of ZB-ZnTe. The Murnaghan relation is based on the assumption of a linear pressure dependence of the bulk modulus $B(P) = B_0 + B'P$. We adopt $B' = 4.7$ (see [15]). The constant m_ξ is different for each RIM parameter. The full set of parameters used in the present work is listed in table 2.

Figure 5 displays the pressure dependence of the phonon frequencies calculated by using the RIM description together with experimental data derived from the Raman spectra. The calculated change in the LA(X) and LA(L) phonon frequencies with pressure (not observed in the Raman spectra) is included in figure 5. The overall good agreement between the RIM frequencies and experimental data is as expected, because the model is fitted to the Raman data. This also applies to the calculated values for the elastic compliances c_{11}, c_{12} and c_{44} at ambient pressure (see table 3). We also list in table 3 the calculated c_{ij} values for ZnTe at 4.5 and 9 GPa. These values could be tested in ultrasonic experiments similar to those recently performed for ZnO up to 8 GPa [44]. Of particular interest would be whether c_{44} remains nearly constant, as in our empirical model, or whether it softens with pressure similar to c_{44} and c_{66} in wurtzite ZnO.

Figure 6 shows the calculated phonon dispersion curves for ZnTe along high-symmetry directions of the BZ at two different pressures (0 and 9 GPa). Although we have slightly modified the RIM parameters to better fit our Raman data, there is good agreement with the neutron scattering data taken from [8] (see figure 6).

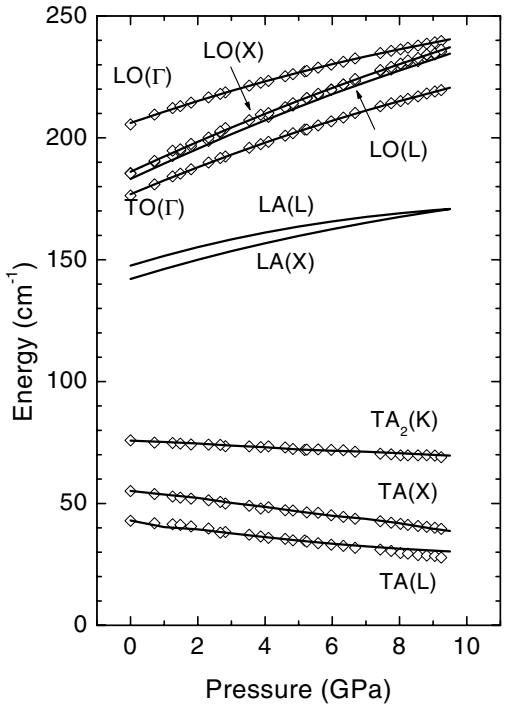

Figure 5. Calculated phonon frequencies of ZB-ZnTe as a function of pressure (solid curves). The mode assignments are indicated. The symbols represent frequency values derived from the experimental Raman spectra. The LO(X) and LO(L) modes are almost degenerate throughout the entire pressure range.

By using the tetrahedron method [45] and taking as input the eigenfrequencies obtained from the RIM calculations we have obtained the one- and two-phonon densities of states (DOSs) shown in figure 7. In the one-phonon DOS, the range corresponding to the TA modes widens with increasing pressure due to the mode softening, while that corresponding to the optical modes narrows, partly due to the decrease of e^* as discussed above. The most pronounced features in the two-phonon DOS are labelled according to the relevant phonon combinations. Below $\sim$200 cm^{-1} ($P = 0$) the two-phonon DOS consists of acoustic phonon combinations only. Features due to the mixed combinations TO + TA(LA) and LO + TA(LA) appear above 215 cm^{-1} at ambient pressure. The frequencies of the first-order TO and LO modes are marked by arrows in figure 7.

3.3. Mode Grüneisen parameters

The Grüneisen parameters γ_i have been calculated for phonons throughout the first BZ using the RIM parameters. Dispersion relations for $\gamma_i(\vec{q})$ at ambient pressure are shown in figure 8 and selected values of the γ_i are listed in table 1. The Grüneisen parameters of all optical phonons and the LA branch are positive and show only small variations (from 1.2 to 2 over the whole BZ), while in the case of the TA phonons there is a larger dispersion with negative values occurring in large regions of the BZ. There is a discontinuity in the Grüneisen parameter γ_{TA} at the Γ-point, the value being positive when it approaches Γ from the [100] direction, while it is close to zero along the Γ–L direction.

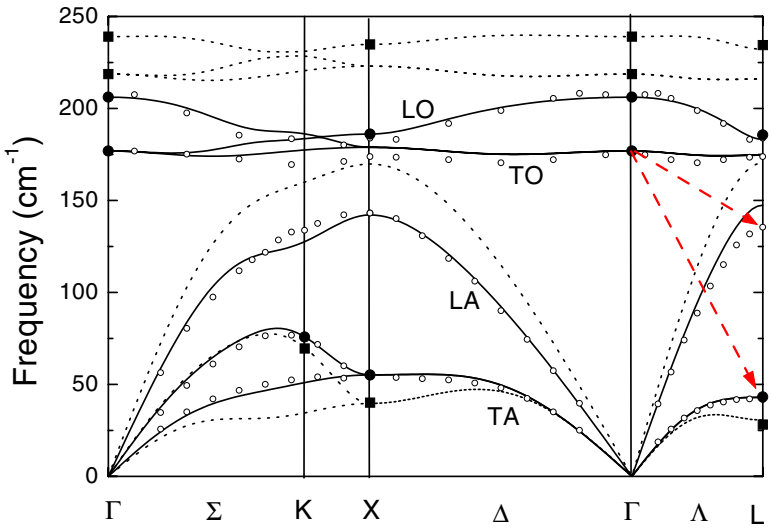

Figure 6. Calculated phonon dispersion relations for ZB-ZnTe at ambient pressure (solid curves) and 9.0 GPa (dotted curves). Closed circles and squares represent the energies of the Raman features observed at 0 and 9 GPa, respectively. The open symbols refer to inelastic neutron scattering data after [8]. The two arrows indicate a possible anharmonic decay process for the zone-centre TO phonons.

The pressure dependence of phonon Grüneisen parameters was addressed recently in several communications [7,46,47]. Using the RIM parameters of table 2, the mode Grüneisen parameters can be calculated as a function of pressure for any wavevector within the BZ. Results for the Γ and X points are shown in figure 9. From the linear or quadratic relations fitted to the experimental Raman frequencies (see table 1) and the linear pressure dependence of the bulk modulus (see above) we derive the variation of the Grüneisen parameters γ_i with pressure represented by symbols in figure 9. The Grüneisen parameters corresponding to the optical modes change very little with pressure. This applies to most of the BZ regions studied. At the Γ point there is a tendency of γ_{LO} and γ_{TO} to decrease as pressure increases. This agrees with observations discussed in [7]. The effect, however, is quite weak (a few per cent) if compared with the changes of acoustic mode Grüneisen parameters, which decrease considerably with pressure. This decrease is very pronounced for the TA(X) and TA(L) modes. For instance, $\gamma_{\mathrm{TA}}(\mathrm{X})$ changes from -1.42 at $P = 0$ to about -4.0 at 9 GPa.

3.4. Thermal expansion under pressure

The negative Grüneisen parameters of the zone-boundary TA modes are responsible for the anomalous negative thermal expansion $\alpha(T)$ of ZnTe at low temperatures [8,48,49]. The TA mode softening and the large changes in TA mode Grüneisen parameters are expected to lead to more pronounced thermal expansion anomalies under pressure. The calculated results for $\gamma_i(\vec{q},\ P)$ throughout the BZ can be used to estimate the temperature dependence of α. The relation for α is

$$\alpha(T) = \frac{N\hbar^2}{3Bv_a kT^2}\int_0^{\omega_{\max}} \mathrm{d}\omega\, \omega^2 n^2(\omega)\mathrm{e}^{\hbar\omega/kT} Z_\gamma(\omega) \tag{5}$$

where N is the total number of cells in the crystal, v_a is the volume of the unit cell, k is the Boltzmann constant and $n(\omega)$ is the average phonon population as given by the Bose–Einstein

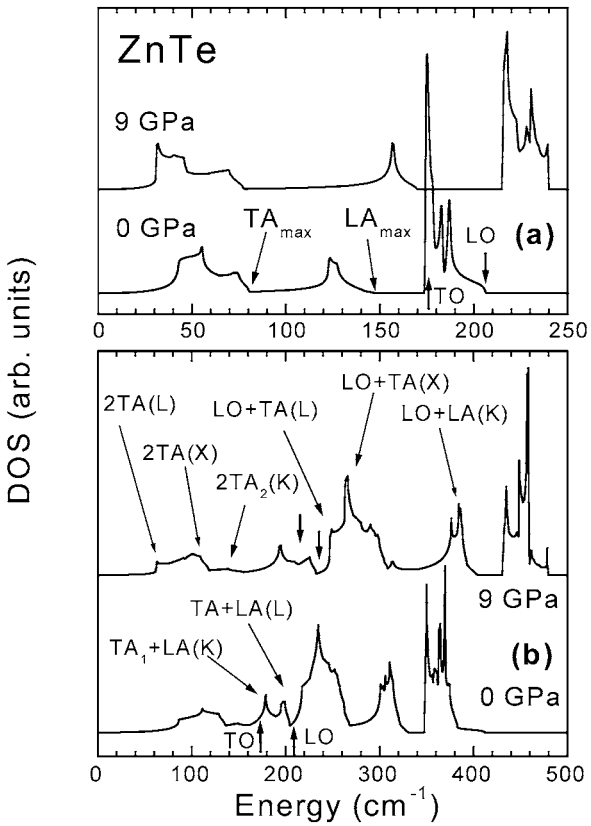

Figure 7. One- and two-phonon densities of states of ZB-ZnTe at ambient pressure and 9 GPa. Pronounced features in the two-phonon DOS are labelled according to the respective phonon combinations. The arrows in (b) labelled TO and LO mark the frequencies of the zone-centre optical phonons.

distribution $n(\omega) = [\exp(\hbar\omega/k_B T) - 1]^{-1}$. We have introduced here the spectral function $Z_\gamma(\omega)$, which represents the density of states normalized to the number of modes, weighted with the Grüneisen parameters:

$$Z_\gamma(\omega) = \frac{1}{N}\sum_{i\vec{q}} \delta(\omega - \omega_i(\vec{q}))\gamma_i(\vec{q}). \tag{6}$$

By again using the tetrahedron method [45] and taking as input, in addition to the eigenfrequencies, the mode Grüneisen parameters obtained from the RIM calculations, we have calculated $\alpha(T)$ at different pressures. Selected results for ambient pressure and 9 GPa are shown in figure 10. Our result matches the ambient-pressure experimental data [50, 51] much better than previous RIM computations [10, 52] or other models [37]. The reason is that we have used here the wavevector-dependent mode Grüneisen parameters $\gamma_i(\vec{q})$, not an average parameter as in earlier calculations. At high pressure (9 GPa) the maximum value of the negative thermal expansion increases by about a factor of two and α is negative over a larger range of temperatures as compared to ambient pressure (see figure 10). This behaviour can be understood by comparing the spectral function $Z_\gamma(\omega)$ at 0 and 9 GPa, plotted as an inset in figure 10. The negative contribution of the TA modes increases with pressure, while the positive contribution of the LA and optic modes decreases. A similar behaviour is expected

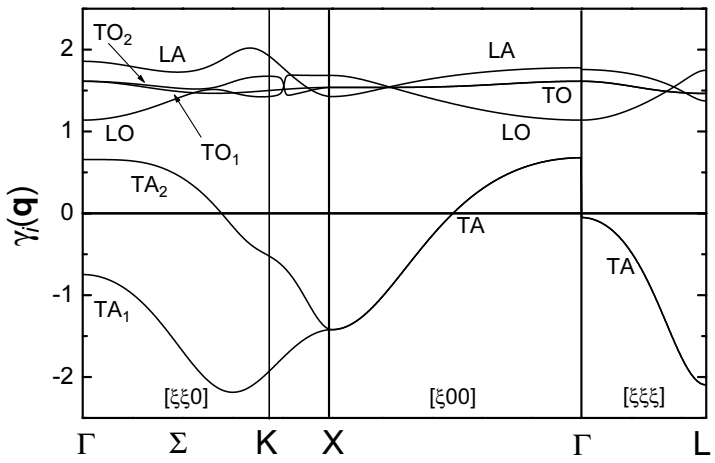

Figure 8. Dispersion of mode Grüneisen parameters at ambient pressure according to the RIM calculations.

for other tetrahedral semiconductors with pronounced TA mode softening under pressure. In this context we refer to [53], where the cases of GaAs and ZnSe have been discussed within the framework of a density functional calculation.

3.5. Raman line widths

In *undoped* semiconductors there are basically two effects which determine the spectral shape of a first-order Raman feature: disorder including that due to isotopic composition [54] and the anharmonic decay into phonons at lower energy (see [55] and citations therein). In the presence of disorder, the $\vec{q} = 0$ selection rule for first-order Raman scattering is not strictly valid. This can lead to a broadening of a Raman line which is partly determined by the dispersion of the corresponding phonon branch. In the case of ZnTe the TO Raman feature may be less affected by disorder than the LO feature because of the smaller dispersion of the TO branches (see figure 6).

In recent low-temperature Raman studies of Si, Ge, CuCl, CuBr and GaP [56–59] it was demonstrated that pressure-induced changes in the TO and/or LO line widths can be well explained by variations in the rate at which zone-centre optical phonons decay into zero-wavevector two-phonon combinations due to third-order anharmonic coupling. The anharmonic line broadening is determined by the imaginary part $\Gamma(\omega)$ of the phonon self-energy, which is proportional to the $\vec{q} = 0$ two-phonon density of states weighted by thermal population factors [55]. Throughout the pressure range from 0 to 9 GPa, the two-phonon DOS is higher at the TO(Γ) frequency than at the LO(Γ) frequency (see arrows in figure 7). In fact, the LO mode frequency always falls into the DOS minimum following after the high-frequency cut-off for TA + LA combinations. Assuming a similar anharmonic coupling strength for the TO and LO modes to the relevant acoustic mode combinations, one would expect a TO line width larger than that of the LO mode, as is observed experimentally (figure 3).

At this point we cannot unambiguously separate the effects of disorder and anharmonicity on the width of the broad TO feature and its pressure dependence. A low-temperature study of the first-order Raman line width of isotopically pure ZnTe as a function of pressure could provide the answer, because in this case the anharmonic decay effects would not be affected by thermal population factors and partly masked by isotopic disorder.

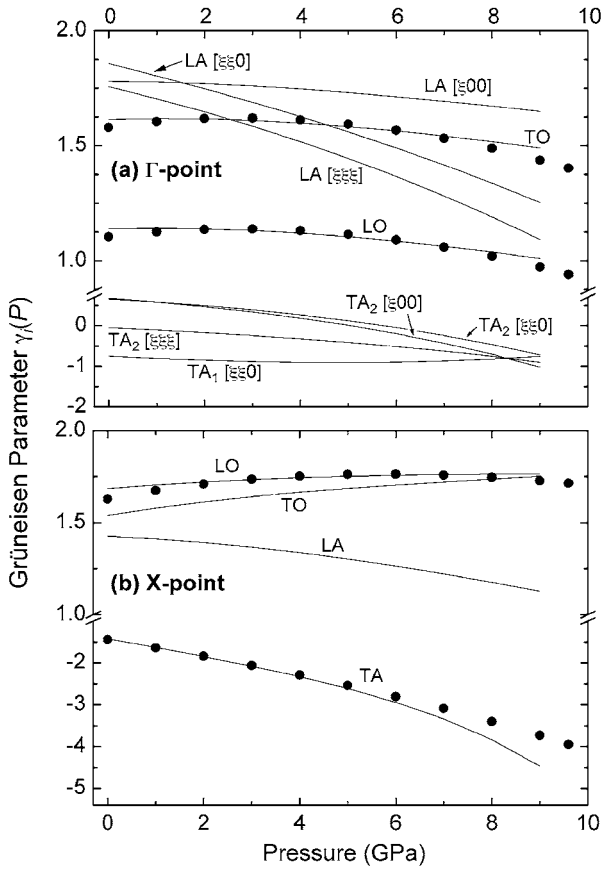

Figure 9. Mode Grüneisen parameters at the Γ and X points of the BZ as a function of pressure. The $\gamma_i(P)$ data (full circles) have been extracted from the experimental data (see text). Solid curves are calculated values using the RIM model.

3.6. Raman intensities

The decrease in intensity of the first-order Raman features with increasing pressure (figures 1 and 4) can be attributed to electronic structure effects [32]. Since we are exciting with red light, we are in the transparent region of the optical spectrum of ZnTe. We may assume that the dominant contribution to the Raman polarizability results from virtual excitations involving the direct optical gap E_g. In this simplified picture the Raman scattering probability $P(\omega_s)$ is [38]

$$P(\omega_s) = I\frac{1}{\hbar\omega_s}\frac{1}{(E_g-\hbar\omega_l)^2(E_g-\hbar\omega_s)^2} \tag{7}$$

where ω_s is the frequency of the scattered light. The prefactor I is proportional to the electron–photon and electron–phonon matrix elements squared. If the increase of the fundamental gap of ZnTe with pressure is taken into account (at 300 K the gap shifts from 2.3 eV at $P = 0$ to 3.0 eV at 9 GPa; see [14, 60–62][4]) we estimate that the energy denominator in equation (7)

[4] According to [5] the bandgap variation at $T = 7$ K and for pressures 0–8 GPa is given by $E(P) = E_0 + aP + bP^2$ with $E_0 = 2.40(1)$ meV, $a = 99.7(5)$ meV GPa^{-1} and $b = -2.3(5)$ meV GPa^{-2}. The values for the linear and quadratic pressure coefficient are nearly identical to those at 300 K reported in [14].

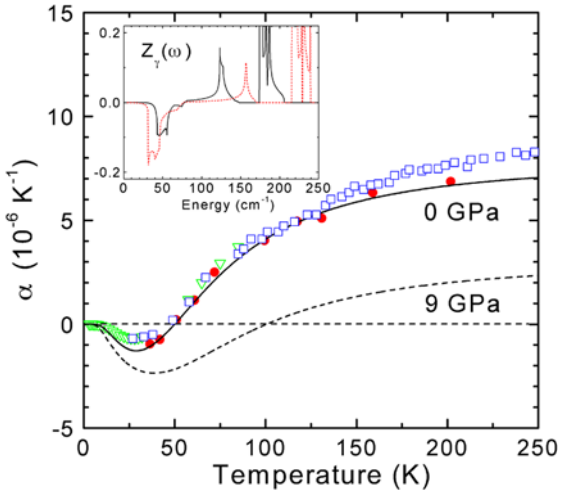

Figure 10. Linear thermal expansion coefficient calculated with the RIM model as a function of temperature at ambient pressure (solid curve) and 9 GPa (dashed curve). The experimental data are taken from [50, 51]. The inset shows the spectral function $Z_\gamma(\omega)$ at 0 GPa (solid curve) and 9 GPa (dashed curve).

increases by a factor of about 50 between 0 and 9 GPa. Thus, considering only the variation of the E_0 gap, the order of magnitude of the observed LO intensity change is reproduced. A more quantitative approach, which is outside the scope of this work, would require the consideration of changes in matrix elements as well as contributions from higher-lying optical gaps. The magnitude of the effect is expected to be different for the TO mode, because in that case we have, in addition to the deformation potential contribution due to the valence band, the Fröhlich interband or electro-optical effect involving the E_0' gap [63]. This effect would change in a non-trivial manner as a function of pressure.

The product of thermal population factors entering the expression for the two-phonon Raman scattering intensity [64] cannot be considered as constant over the pressure range of interest here. This applies in particular to the low-frequency acoustic mode combinations, because, in relative terms, the mode frequencies soften considerably with pressure. Based on the experimental frequency shift of the TA(X, L) modes, we estimate that at 300 K the thermal population effects enhance the 2TA scattering at 9 GPa by roughly a factor of two compared to ambient pressure. This effect is not sufficient to explain the observed intensity increase with pressure. The remaining difference in the acoustic region (mainly for the 2TA feature at X) cannot be explained by 'resonance' effects, i.e. by changes in energy denominators of second-order processes. Instead, the origin seems to be partly in the change of intervalley deformation potentials (matrix element in the scattering process) with pressure [32].

4. Raman spectra of high-pressure phases

Figure 11 shows the Raman spectra measured in the pressure range above the stability limit of the ZB phase, which is 9.6(3) GPa in our Raman experiments. The bottom spectrum in figure 11 corresponds to the ZB phase. There are two pressure regimes, between 10 and 12.2 GPa and above ∼13.7 GPa, each with clearly different Raman spectra. A third regime between 12.2 and 13.7 GPa shows additional Raman features not seen in the other two pressure ranges. This is more evident in a plot of Raman frequencies versus pressure as shown in figure 12.

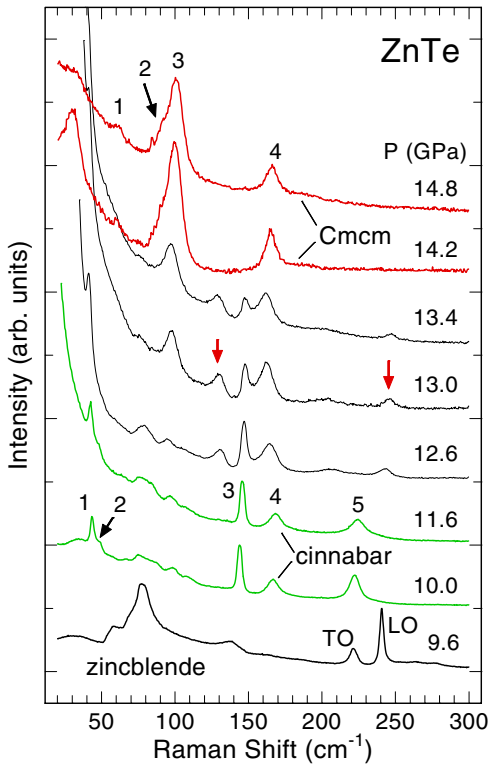

Figure 11. Raman spectra of high-pressure phases of ZnTe at different pressures. All spectra were taken for increasing pressure and the laser wavelength was 647.088 nm. Spectra are for the ZB (9.6 GPa), cinnabar (10.0 and 11.6 GPa) and *Cmcm* phases (14.2 and 14.8 GPa). In the transition regime from cinnabar to *Cmcm* (spectra at 12.6, 13.0 and 13.4 GPa) there appear Raman features (some marked by arrows), which indicate the possible existence of a new intermediate phase.

The first region (9.6–12.2 GPa) corresponds to the stability range of the cinnabar phase of ZnTe [21]. For a cinnabar-type structure (space group D_3^4, $P3_121$, $Z = 3$) there are altogether 18 zone-centre modes [65]

$$2A_1 + 4A_2 + 6E.$$

The A_1 and the E modes are Raman active whereas the A_2 modes are Raman forbidden. One A_2 and one of the twofold degenerate E modes are the acoustic ones. Thus, we expect up to 12 first-order Raman features. We can clearly identify five peaks in the relevant pressure range. At 10.8 GPa their frequencies are 43, 49, 145, 168 and 234 cm^{-1}. Since the ZB phase shows strong second-order scattering, some additional Raman features of the cinnabar phase at frequencies between 60 and 120 cm^{-1} may be due to scattering by combination modes.

According to x-ray diffraction results [22], the cinnabar phase of ZnTe transforms to the *Cmcm* phase at about 12 GPa and the stability range of that phase extends to at least 85 GPa. It is therefore reasonable to assume that the Raman spectra measured above 13.7 GPa are for the *Cmcm* phase. The *Cmcm* structure is a distorted variant of the rocksalt structure. The effective atom coordination is between five and six as compared with four in the cinnabar phase. For the *Cmcm* phase (D_{2h}^{17}, $Z = 2$) there are altogether 12 modes

$$2A_g + 2B_{1g} + 2B_{1u} + 2B_{2u} + 2B_{3g} + 2B_{3u}$$

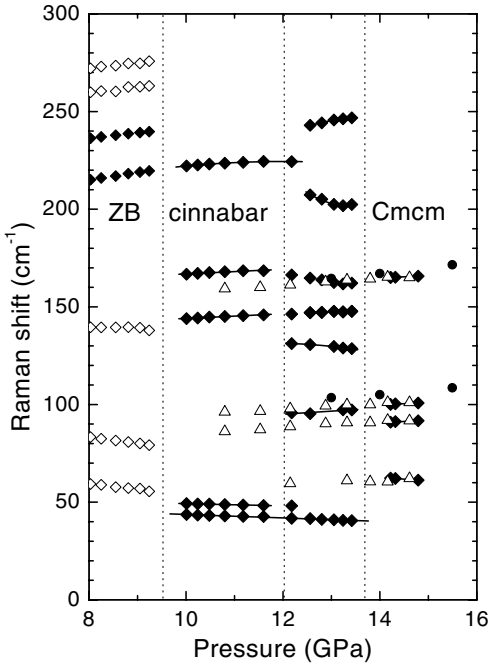

Figure 12. Observed Raman frequencies of high-pressure phases of ZnTe as a function of pressure. Open triangles refer to data obtained on releasing pressure. The dashed lines at 12 and 13.7 GPa mark the transition regime from the cinnabar to the *Cmcm* phase. In this regime some other phase possibly coexists with cinnabar and (or) *Cmcm*.

of which the six *gerade* modes are Raman active (three of the *ungerade* modes are acoustic ones). In the Raman spectra we observe at least four features. At 14.8 GPa their frequencies are 61, 92, 101 and 166 cm^{-1}. In contrast to the cinnabar phase, which is semiconducting with an optical gap near 2.5 eV [13, 14], the *Cmcm* phase of ZnTe is metallic [13, 14, 24, 25]. According to band structure calculations [29, 30], the metallic character arises from a small overlap (1 eV) between valence and conduction bands. The presence of free carriers does not preclude the detection of phonon Raman signals.

The assignment of the Raman features in the cinnabar and *Cmcm* phases is uncertain at this point. Calculations of zone-centre phonon frequencies for these phases are under way in order to support tentative assignments not discussed here.

In the intermediate-pressure region, from approximately 12.2 to 13.7 GPa, some of the Raman peaks seem related to those of the cinnabar or *Cmcm* phases, based on similar Raman frequencies (see figure 12). However, additional Raman features observed in this range indicate the possible existence of an as yet unknown phase of ZnTe. The fact that such a phase was not detected in diffraction experiments may be due to a coarse pressure scanning, but different stress or sample conditions in the Raman and diffraction experiments (e.g. single-crystal versus polycrystalline starting material) could also affect the appearance of a phase with marginal stability relative to neighbouring phases.

One of the Raman modes indicating an intermediate phase has a frequency near 250 cm^{-1}, which is about as large as the LO mode frequency of the ZB phase at 9 GPa. A possible structure candidate for an intermediate phase is the SC16 structure (space group $Pa\bar{3}$, $Z = 8$) which represents a distorted tetrahedral network and occurs for stable or metastable high-pressure

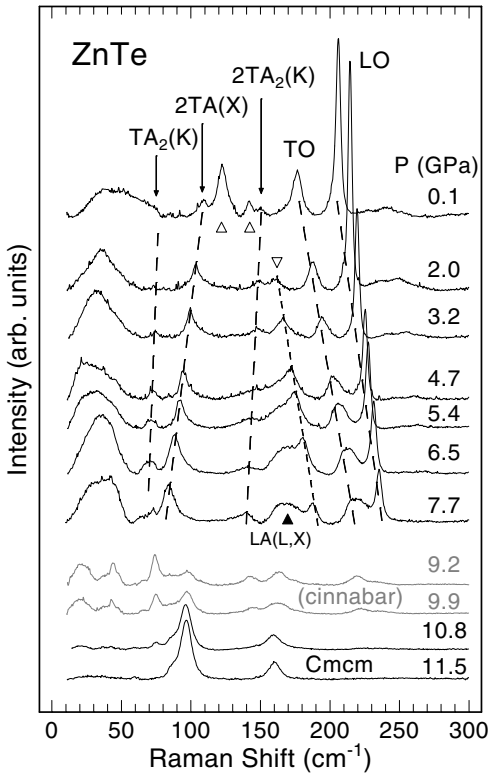

Figure 13. Raman spectra of ZnTe measured for decreasing pressure starting with the *Cmcm* phase. This phase is seen down to at least 10 GPa. Features characteristic of the ZB phase (connected by dashed lines, also marked by arrows) reappear at around 8 GPa. See text for comments on additional features marked by open triangles.

phases in other polar semiconductors, for example CuCl, CuBr and GaAs [66]. In the case of CuCl and CuBr, the highest-frequency Raman modes in the SC16 phases occur above or near the extrapolated LO mode frequencies of the ZB phases [67, 68].

In this context we note that in recent theoretical work on the phase stability of ZnS and ZnSe under pressure the authors suggest a narrow stability range for the SC16 structure intermediate between the ZB and high-pressure rocksalt phases [69]. It should also be mentioned that very recently the cinnabar phase was actually observed in ZnSe after first transforming to the rocksalt phase and then releasing the pressure [70]. Thus, the combined experimental and theoretical results point to a near-degeneracy of the total energies of cinnabar and SC16 in ZnSe. A similar situation may be present in ZnTe. To our knowledge, the possible stability of the SC16 structure of ZnTe has not yet been explored using total energy calculations.

In the Raman spectra measured for releasing pressure (figure 13) all features characteristic of the *Cmcm* phase are observed down to at least 10 GPa. The spectra can be interpreted in terms of a reappearance of the cinnabar phase between 10 and 8 GPa. The TO and LO peaks characteristic of ZB reappear near 8 GPa and ZB is the majority phase present upon fully releasing the pressure. The assignment of some spectral features marked by open triangles in figure 13 is not clear. These could be difference modes or arise from an admixture of a metastable phase. A possible candidate is the wurtzite modification of ZnTe, because this phase is expected to be close in total energy to the ZB phase [28].

5. Summary

Raman spectra of ZB-ZnTe were measured under hydrostatic pressure ($T = 300$ K) up to about 9.6 GPa, where the transition to the cinnabar phase occurred in our experiments. Experimental mode Grüneisen parameters were obtained for the first-order Raman modes and a few other Raman features involving two-phonon combinations at critical points of the BZ. We have extracted the pressure dependence of the transverse dynamic effective charge from that of the LO–TO mode splitting. Furthermore, a RIM description of phonon frequencies of ZnTe has been fitted to the pressure-dependent Raman data. The model is used to calculate the pressure-dependent dispersions of mode Grüneisen parameters throughout the BZ. These results then enter our calculation of the temperature dependence of the linear thermal expansion. At ambient pressure the $\alpha(T)$ behaviour, in particular the negative α values at low temperatures, is very well reproduced and it is in much better agreement with experiment than previous attempts to calculate $\alpha(T)$ for ZnTe. We demonstrate that the temperature region of negative expansion should increase with increasing pressure. The physical reason mainly lies in negative values of the TA mode Grüneisen parameters. The one- and two-phonon DOSs obtained from the RIM description form a basis for a qualitative discussion of the pressure-dependent widths of the first-order TO and LO Raman features. These results could be useful when studying the pressure-dependent phonon lifetimes in ZnTe at low temperatures.

Raman spectra of the high-pressure cinnabar and $Cmcm$ phases of ZnTe are reported. The data for the high-pressure phases could be used as reference points when modelling the phonon dispersions using, for instance, linear response theory. Based on the present results we suggest checking for the possible existence of a phase intermediate between cinnabar and ZB modifications, by diffraction experiments or *first-principles* total energy calculations.

Acknowledgments

Our thanks are due to C Abraham, who participated in preliminary work on the Raman scattering of ZnTe under pressure. We thank W Dietrich, U Oelke and U Engelhardt for technical assistance. JC acknowledges financial support from the Ministerio de Educación, Cultura y Deportes (Spain) and the Max-Planck-Gesellschaft (Germany).

References

[1] For a collection of recent reviews see Suski T and Paul W (ed) 1998 High pressure in semiconductor physics I and II *Semiconductors and Semimetals* vol 54 and 55 (New York: Academic)
[2] Mitra S S, Brafman O, Daniels W B and Crawford R K 1969 *Phys. Rev.* **186** 942
[3] Brafman O and Mitra S S 1971 *Light Scattering in Solids* ed M Balkanski (Paris: Flammarion) p 284
[4] Weinstein B A 1976 *Proc. 13th Int. Conf. on the Physics of Semiconductors (Rome, 1976)* ed F G Fumi p 326
Weinstein B A 1977 *Solid State Commun.* **24** 595
[5] Abraham C 1992 *PhD Thesis* Univ. Stuttgart
[6] Thomas R J, Boley M S, Chandrasekhar H R, Chandrasekhar M, Parks C, Ramdas A K, Han J, Kobayashi M and Gunshor R L 1994 *Phys. Rev.* B **49** 2181
[7] Frogley M D, Dunstan D J and Palosz W 1998 *Solid State Commun.* **107** 537
[8] Vagelatos N, Wehe D and King J S 1974 *J. Chem. Phys.* **60** 3613
[9] Plumelle P and Vandevyver M 1976 *Phys. Status Solidi* b **73** 271
[10] Talwar D N, Vandevyver M, Kunc K and Zigone M 1981 *Phys. Rev.* B **24** 741
[11] Samara G A and Drickamer H G 1962 *J. Phys. Chem. Solids* **23** 124
[12] Smith P L and Martin J E 1965 *Phys. Lett.* **19** 541
[13] Ohtani A, Motobayashi M and Onodera A 1980 *Phys. Lett.* A **75** 435
[14] Strössner K, Ves S, Kim C K and Cardona M 1987 *Solid State Commun.* **61** 275

[15] Strössner K, Ves S, Hönle W, Gebhard W and Cardona M 1987 *Proc. 18th Int. Conf. on Physics of Semiconductors* ed O Engström (Singapore: World Scientific) p 1717
[16] San Miguel A, Polian A, Itie J P, Marbeuf A and Triboulet R 1992 *High Pressure Res.* **10** 412
[17] Qadri S B, Skelton E F, Webb A W and Hu J Z 1994 *High Pressure Science and Technology (AIP Conf. Proc. vol 309)* p 319
[18] Kusaba K and Weidner D J 1994 *High Pressure Science and Technology (AIP Conf. Proc. vol 309)* p 553
[19] McMahon M I, Nelmes R J, Wright N G and Allen D R 1994 *High Pressure Science and Technology (AIP Conf. Proc. vol 309)* p 633
[20] San Miguel A, Polian A, Gautier M and Itie J P 1993 *Phys. Rev.* B **48** 8683
[21] Nelmes R J, McMahon M I, Wright N G and Allan D R 1995 *J. Phys. Chem. Solids* **56** 545
[22] Nelmes R J, McMahon M I, Wright N G and Allan D R 1994 *Phys. Rev. Lett.* **73** 1805
[23] Nelmes R J and McMahon M I 1998 *High Pressure in Semiconductor Physics* vol 1, ed T Suski and W Paul (New York: Academic) p 146
[24] Wang Z and Syassen K unpublished work cited in Suski T and Paul W (eds) 1998 *High Pressure in Semiconductor Physics* vol 1 (New York: Academic) p 387
[25] Goñi A R and Syassen K 1998 *High Pressure in Semiconductor Physics* vol 1, ed T Suski and W Paul (New York: Academic) p 248
[26] Kobayashi M 2001 *Phys. Status Solidi* b **223** 55
[27] Shimomura O, Utsumi W, Urakawa T, Kikegawa T, Kusaba K and Onodera A 1997 *Rev. High Pressure Sci. Technol.* **6** 702
[28] Yeh C Y, Lu Z W, Froyen S and Zunger A 1992 *Phys. Rev.* B **46** 10 086
[29] Lee J D and Ihm J 1996 *Phys. Rev.* B **53** R7622
Lee G D, Hwang C D, Lee M H and Ihm J 1997 *J. Phys.: Condens. Matter* **9** 6619
[30] Cote M, Zakharov O, Rubio A and Cohen M L 1997 *Phys. Rev.* B **55** 13 025
[31] Piermarini G J, Block S, Barnett J P and Forman R A 1975 *J. Appl. Phys.* **46** 2774
Mao H K, Xu J and Bell P M 1986 *J. Geophys. Res.* **91** 4673
[32] Schmidt R L, McCombe B D and Cardona M 1975 *Phys. Rev.* B **11** 746
[33] Weinstein B A and Zallen R 1984 *Light Scattering in Solids* vol 4, ed M Cardona and G Güntherodt (Berlin: Springer) p 463
[34] Anastassakis E and Cardona M 1998 *High Pressure in Semiconductor Physics* vol 2, ed T Suski and W Paul (New York: Academic) p 152
[35] Xu C H, Wang C Z, Chan C T and Ho K M 1991 *Phys. Rev.* B **43** 5024
[36] Lee B H 1970 *J. Appl. Phys.* **41** 2988
[37] Soma T 1980 *Solid State Commun.* **34** 927
[38] Yu P Y and Cardona M 1998 *Fundamentals of Semiconductor Physics* (Berlin: Springer)
[39] Olego D, Cardona M and Vogl P 1982 *Phys. Rev.* B **25** 3878
Karch K and Bechstedt F 1996 *Phys. Rev. Lett.* **77** 1660
[40] Goñi A R, Siegle H, Syassen K, Thomsen C and Wagner J-M 2001 *Phys. Rev.* B **64** 035205
[41] Kunc K 1973–1974 *Ann. Phys., NY* **5** 319
Kunc K 1973 *PhD Thesis* Université de Paris VI
[42] Eryigit R and Herman I P 1996 *Phys. Rev.* B **53** 7775
[43] Murnaghan F D 1944 *Proc. Natl Acad. Sci. USA* **30** 244
[44] Decremps F, Zhang J, Li B and Liebermann R C 2001 *Phys. Rev.* B **63** 224105
[45] Lehmann G and Taut M 1972 *Phys. Status Solidi* b **54** 469
[46] Liu L 2000 *Solid State Commun.* **114** 637
[47] Wagner J-M 2000 *Solid State Commun.* **116** 355
[48] Soma T 1977 *J. Phys. Soc. Japan* **42** 1491
[49] Soma T and Kudo K 1980 *J. Phys. Soc. Japan* **48** 115
[50] Novikova S I and Abrikosov N Kh 1964 *Sov. Phys.–Solid State* **5** 1558
[51] Collins J G, White G K, Birch J A and Smith T F 1980 *J. Phys. C: Solid State Phys.* **13** 1649
[52] Vetelino J F, Mitra S S and Namjoshi K V 1970 *Phys. Rev.* B **2** 967
[53] Debernardi A and Cardona M 1996 *Phys. Rev.* B **54** 11 305
[54] Göbel A, Ruf T, Zhang J M, Lauck R and Cardona M 1999 *Phys. Rev.* B **59** 2749
[55] Debernardi A 2000 *Solid State Commun.* **113** 1 and references therein
Debernardi A, Baroni S and Molinari E 1995 *Phys. Rev. Lett.* **75** 1819
[56] Ulrich C, Anastassakis E, Syassen K, Debernardi A and Cardona M 1998 *Phys. Rev. Lett.* **78** 1283
[57] Ulrich C, Göbel A, Syassen K and Cardona M 1999 *Phys. Rev. Lett.* **82** 351
[58] Ves S, Loa I, Syassen K, Widulle F and Cardona M 2001 *Phys. Status Solidi* b **223** 241

[59] Manjón F J, Serrano J, Loa I, Syassen K, Lin C T and Cardona M 2001 *Phys. Status Solidi* b **223** 331
[60] Weinstein B A, Zallen R, Slade M L and deLonzanne A 1981 *Phys. Rev.* B **24** 4652
[61] Lindner M, Schötz G F, Link P, Wagner H P, Kuhn W and Gebhardt W 1992 *J. Phys.: Condens. Matter* **4** 6401
[62] Reimann K, Haselhoff M, Rubenacke S and Steube M 1996 *Phys. Status Solidi* b **198** 71
[63] Cardona M 1982 *Light Scattering in Solids* vol 2, ed M Cardona and G Güntherodt (Heidelberg: Springer) p 19
[64] Zeyher R 1974 *Phys. Rev.* B **9** 4439
[65] Imaino W, Simpson C T, Becker W M and Ramdas A K 1980 *Phys. Rev.* B **21** 634 and references therein
[66] Hull S and Keen D A 1994 *Phys. Rev.* B **50** 5868
McMahon M I, Nelmes R J, Allen D R, Belmonte S A and Bovornratanaraks T 1998 *Phys. Rev. Lett.* **80** 5564
[67] Ulrich C, Syassen K, Cardona M, Cros A and Cantarero A 1999 *Phys. Rev.* B **60** 9410
[68] Manjon F J, Serrano J, Loa I, Syassen K, Lin C T and Cardona M 2001 *Phys. Rev.* B **64** 064301
[69] Qteish A and Parrinello M 2000 *Phys. Rev.* B **61** 6521
Qteish A and Muñoz A 2000 *J. Phys.: Condens. Matter* **12** 1705
Qteish A and Muñoz A 2001 *Phys. Status Solidi* b **223** 417
[70] Kasaba K and Kikegawa T 2000 Poster presented at the *3rd Int. Workshop on Crystallography at High Pressure and High Temperature Using X-Rays and Neutrons, SPring-8 (2000)*
Pellicer-Porres J *et al* 2001 *Abstract 39th EHPRG Meeting (Santander, 2001)*